Clogging detection and productive layers identification along boreholes using Active Distributed Temperature Sensing

Jeremy Godinaud, Maria Klepikova, F. Larroque, Nicolas Guihéneuf, A. Dupuy, Olivier Bour

To cite this version:

Jeremy Godinaud, Maria Klepikova, F. Larroque, Nicolas Guihéneuf, A. Dupuy, et al.. Clogging detection and productive layers identification along boreholes using Active Distributed Temperature Sensing. Journal of Hydrology, 2023, 617 (Part C), pp.129113. 10.1016/j.jhydrol.2023.129113 . insu-03955737

HAL Id: insu-03955737
https://insu.hal.science/insu-03955737v1

Submitted on 20 Feb 2023

Highlights

Clogging detection and productive layers identification along boreholes using Active Distributed Temperature Sensing

J.Godinaud, M.Klepikova, F.Larroque, N.Guihéneuf, A.Dupuy, O.Bour

- Active Distributive Thermal Sensing experiment achievement at ATES site
- Determination of thermal conductivity and groundwater flux along boreholes
- Identification of clogging location along boreholes

Clogging detection and productive layers identification along boreholes using Active Distributed Temperature Sensing

J.Godinaud[a], M.Klepikova[b], F.Larroque[a], N.Guihéneuf[b], A.Dupuy[a], O.Bour[b]

[a]*ENSEGID Bordeaux INP, CNRS, EPOC UMR 5805, Pessac, 33600, France*
[b]*Univ Rennes, CNRS, Geosciences Rennes - UMR 6118, Rennes, 35000, France*

Abstract

Fiber-Optic Active Distributed Temperature Sensing (FO-ADTS) experiments were performed on an Aquifer Thermal Energy Storage system (ATES) site located on the university campus of Bordeaux, France. The experiments consisted in heating the steel core of the FO cable while monitoring the rate of temperature increase during the heating periods. The changes in temperature, that were monitored through time at every depth under various hydraulic conditions and in different boreholes, were used to evaluate both aquifer properties and wells conditions. A first ADTS experiment was conducted under cross borehole configuration using a pumping well and a monitoring well separated by a distance of 8.5 meters. Then, to check the reciprocity of the results, a second experiment was conducted by switching the monitoring and the pumping well. The results obtained through the use of analytical solutions for reproducing and interpreting the data lead to the following conclusions: (i) ADTS can be used to estimate both thermal conductivity and Darcy velocity distribution along boreholes, crucial properties for ATES performance. (ii) The proposed method is a promising tool to detect clogging locations in the boreholes when it occurs. This can be of great practical interest to maintain systems performance, since, once FO cables deployed, experiments could be easily repeated without opening boreholes and stop the system operation.

Keywords:
Distributed Temperature Sensing, Groundwater Flux, Thermal Conductivity, Clogging, ATES

---

1. Introduction

Aquifer Thermal Energy Storage (ATES) is an open loop geothermal system involving at least two reversible boreholes [Fleuchaus et al., 2018]. This technology uses the subsurface as transient long-term storage of cold and warm water and it gains more and more popularity with a great potential to reduce green house gas emissions of the building sector [Vanhoudt et al., 2011, Gao et al., 2017, Ghaebi et al., 2017, Schüppler et al., 2019, Stemmle et al., 2021].

ATES performance is highly sensitive to hydrogeological conditions. It requires good aquifer permeability to pump and inject water into the aquifer, low natural groundwater flow to avoid stored energy losses due to advection and/or thermal interaction between wells. During system operation, storage efficiency and energy recovery rate depend on the cold and warm thermal plumes extension [Bloemendal and Hartog, 2018]. The spatiotemporal distribution of temperature is particularly impacted by aquifer heterogeneity especially regarding the groundwater flux and thermal properties distribution [Ferguson, 2007, Sommer et al., 2013, Bridger and Allen, 2014, Ganguly and Mohan Kumar, 2014, Possemiers et al., 2015, Visser et al., 2015, Nguyen et al., 2016, Bloemendal and Hartog, 2018].

ATES performance also depends on wells sustainability which can be impacted by their aging. Among the main issues, corrosion, biological, chemical and physical clogging are major problems which could lead to well damages and performance decrease [Fleuchaus et al., 2018, Bloemendal and Olsthoorn, 2018]. The causes and consequences of the boreholes clogging are well documented for open loop systems [Bakema, 2001, Song et al., 2020]. A large clogging development is an additional source of geothermal system performance decrease. Quantification of the subsurface heterogeneity, and the surveillance of clogging evolution in wells, are therefore major concerns on ATES site.

Classically, thermal and hydrodynamic properties of aquifers are characterized from laboratory measurements on core samples. Moreover, some field surveys may be used in the context of ATES characterization. Among these surveys, pumping tests give an average value of aquifer transmissivity and specific storage. Their monitoring time ranges classically between 1 and 3 days and their well known interpretation provides a first overview of hydrogeological properties and context of a site [Kruseman and Ridder, 1994]. Flowmeter logs are suited to obtain the vertical flow distribution at a particular point and can provide information on fracture connectivity, transmissivity and storativity distribution [Molz et al., 1994, Paillet, 1998, Roubinet et al., 2015]. These tests are simple to realize and can be performed in short time. Heat or solute tracer tests are used to investigate groundwater velocity, thermal and hydraulic dispersivity, or location of preferential groundwater paths [Bodin et al., 2003, Klepikova et al., 2016, Irvine et al., 2015]. But they are more difficult to realize, and a robust interpretation could require a lot of observation points, as well as comprehensive numerical modeling. Thermal Response Tests (TRT) are used to estimate the average thermal conductivity of aquifers at the vicinity of the tested well, but the data collection could require a long time [Beier et al., 2011, Dong et al., 2022]. Finally, cores collection is financially costly, time-consuming, and their analysis provides only local information which could not be representative of the global in-site aquifer dynamics [Sharqawy et al., 2013].

Preventive actions to tackle clogging development include reduction in the frequency of pump starts and stops, underground removal of iron, avoiding possible oxygen infiltration or reduction of water turbidity and organic content. Nevertheless, a certain clogging extension cannot be avoided during the recharge process, thus leading to the decrease of geothermal system performance [Song et al., 2020]. Surveillance of the clogging evolution is thus a major challenge for ATES systems, and developing adapted countermeasures on site could significantly help to maintain their performance. Recently, a strategy was developed to follow its evolution [Gjengedal et al., 2020]. The surveillance procedure aims to conduct a step-test with incremental increases in the groundwater flow rate while measuring the pressure and temperature responses in the system components. Nevertheless, it does not focus on clogging locations in the well, but gives an overall view of each component of the geothermal system (production wells, submersible pump and groundwater heat exchanger).

Distributive Thermal Sensing with Fiber Optic cable (FO-DTS) opens a timely opportunity to improve our understanding of the functioning of ATES systems. This technology enables to collect efficiently long data set and to monitor dynamics process [Bense et al., 2016]. For geothermal application, it was first used to monitor temperature variations along production boreholes [Hurtig et al., 1996]. DTS methods have seen further improvements with the use of the active mode (ADTS). It consists on deploying a heat source in the well and monitoring the induced temperature changes [Bense et al., 2016]. The temperature elevation induced by the heat source and the subsequent cooling directly depends on thermal properties of the porous media and on water flux dissipating heat by advection. Among other, it can be used to achieve Enhanced Thermal Response Test (ETRT) to establish thermal conductivity profile for Borehole Heat Exchanger (BHE) application [Freifeld et al., 2008, Huber and Arslan, 2012, Vélez Márquez et al., 2018, Zhang et al., 2020, Hakala et al., 2022]. Furthermore, the method proved its ability to measure groundwater flux distribution in the subsurface [Read et al., 2014, Bakker et al., 2015, des Tombe et al., 2019]. Recent laboratory and field experiments demonstrate that analytical methods can be used to inspect the distribution of thermal conductivity and Darcy velocity along a fiber positioning in saturated porous media [Simon et al., 2021, del Val et al., 2021]. These works enable the generalization of ADTS experiments interpretation.

Apart from aquifer thermal properties, the thermal conductivity profile established in a borehole could be also of major interest to inspect eventual low anomalies due to clogging development. Indeed, the value of thermal conductivity for clogging materials such as bentonite, clay or porous iron hydroxides provides a particular low signature useful for identification [Tang et al., 2008, Cho et al., 2008, Gjengedal et al., 2020, Dalla Santa et al., 2020].

To our knowledge, FO-ADTS experiments in boreholes have never been performed with a purpose of detecting both clogging development and productive layers. Most of the experiments achieved in boreholes mainly focus on fractured zone identification [La Bernardie et al., 2018, Maldaner et al., 2019, Klepikova et al., 2022], Darcy velocity estimation [Selker and Selker, 2018, del Val et al., 2021] or aquifer thermal conductivity [Zhang et al., 2020, Hakala et al., 2022].

In this context, a cross-borehole ADTS experiment was carried out on a site located at the university of Bordeaux in France, and planned to be exploited by a new ATES. The test was realized under constant pumping rate condition and replicated in two different boreholes to verify the reciprocity of the data. The main objectives were **(i)** to characterize the vertical distributions of thermal conductivity and Darcy velocity in two different boreholes, **(ii)** to reveal the preferential water pathways during injection **(iii)** to demonstrate the potential of ADTS to detect clogging area along well screens.

2. Experimental Site

2.1. Context

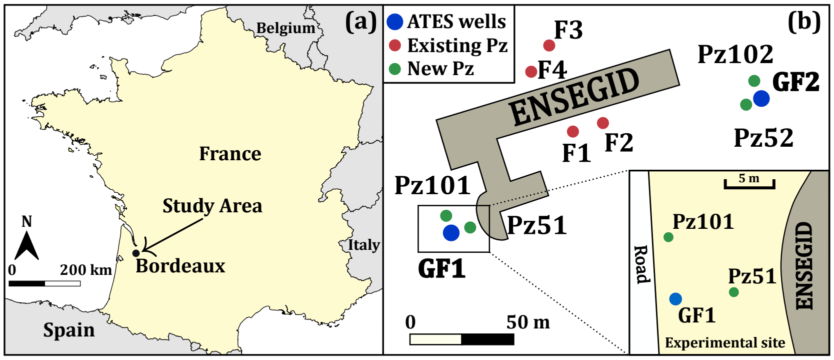

Figure 1: (a) Location of experimental area, (b) ENSEGID site map with boreholes location and focus on the experimental area

The study area is located at the university of Bordeaux (Pessac, France, (Figure 1a), on the site of the Ecole Nationale Superieure en Environnement Georessources et Ingéniérie du Developpement Durable (ENSEGID). An ATES system was designed to supply both cooling and heating to a new building of 3600 m^2. The ATES consists of a pair of 70 m deep reversible pumping/injection wells, GF1 hot well and GF2 cold well, located 145 meters apart (Figure 1b). In addition to the production wells, four piezometers (Pz51, Pz101, Pz52 and Pz102) were created close to the main wells to monitor thermal plume extension and to control piezometric heads. Piezometers

Pz101 and Pz51 are used for the ADTS experiment. They are separated by a distance of 8.5 m and located 6.0 m and 6.5 m apart from the ATES hot production well GF1 . They were drilled to 66 m and 70 m deep respectively. Our experiments were achieved 8 months before the beginning of ATES operation.

Located in the North Aquitaine Basin, the experimental site corresponds to a large multi-layered aquifer system. The actual structure of this basin is the result of Pyrenees retro-foreland basin developed from the Campanian to the Miocene [Labat et al., 2021]. The local geology corresponds to the top of the system formed by a succession of sedimentary deposits during multiple transgression/regression periods, leading to a vertical heterogeneous sequences of limestone, sandstone and clay from Eocene to Plio Quaternary times [Larroque et al., 2013]. The proximal shore location of the site during Oligocene period results in highly horizontally and vertically heterogeneous limestone deposits [Sztrákos and Steurbaut, 2017]. A part of the Oligocene formation, composed by highly porous and permeable fossiliferous limestones, constitutes the ATES aquifer target. Around the experimental site, the deep aquifer is confined, as pointed out by seasonal artesianism. Near the surface level, a 10 meters thick unconfined aquifer, made of Plio Quaternary sand and clay deposits, covers the Oligocene formation. At the site location, the Oligocene aquifer limestone is crossed from 12 m depth to 68 m depth.

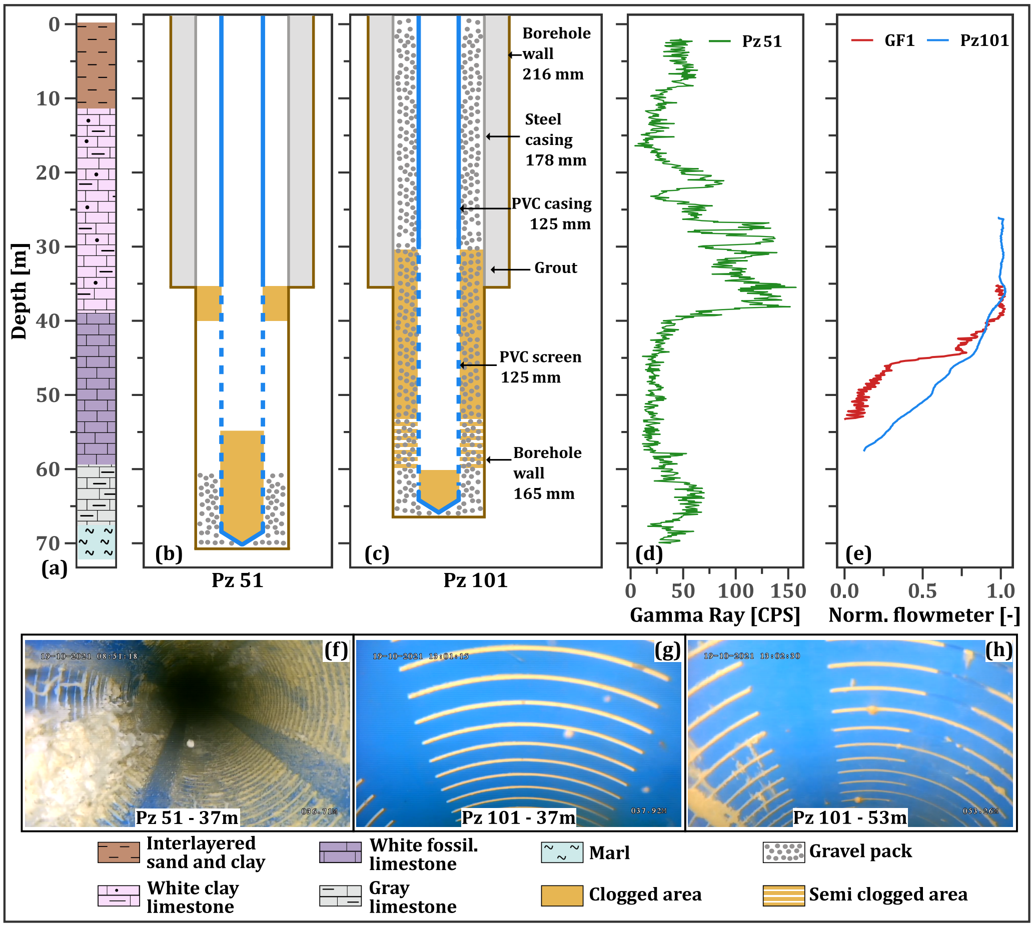

Figure 2: Field data : (a) Geological section of the site, (b) and (c) technical logs of piezometers with clogged area detect during video inspection, (d) Pz51 gammma ray, (e) GF1 and Pz101 flowmeter logs, and (f,g,h) video inspection screenshots

2.2. Field data

The available field data, including gamma ray log, flowmeter logs and drill cuttings observations, highlight a heterogeneous limestone aquifer with a vertical and horizontal unequal distribution of incoming water fluxes. The layer crossed between the depth of 40–60 m (Figure 2a), is made of fossiliferous white limestone. A developed porosity is identified from microscopic drill cuttings observation. In this layer, the Pz51 Gamma Ray values fluctuate around an average of 25.0 cps, which indicates a low clay content (Figure 2d). The GF1 flowmeter reveals that the incoming water is located from the depth of 40 m to 55 m. In this area, a layer of 2 meters thick between the depth of 44 m and 46 m produces about the half of the total discharge (Figure 2e). Another flowmeter realized in Pz101 one year after the end of borehole works completion (and before the beginning of ATES operation) indicates a more homogeneous flux distribution along this borehole (Figure 2e). Between the depth of 60 m and 67 m, the drill cuttings observations emphasize gray limestones, a less developed porosity and a significant clay content. From 67 m, to 71 m, blue marl is encountered. A mean transmissivity value of $7.0 \times 10^{-4}\,\mathrm{m}^2\,\mathrm{s}^{-1}$ is estimated from a two days pumping test in GF1.

Borehole camera inspections show the presence of clogging material in piezometers Pz101 and Pz51 (Figure 2f, g and h). From the depth of 35 m to 39 m, the Pz51 screens are totally clogged by a mix of yellow brown bentonite clay/mud and white bio-fouling bacteria (Figure 2f). The screens are clean in the interval length 40–54 m. The Pz51 bottom is filled with clay and bentonite and encountered at the depth of 54.5 m instead of the 71 m initially drilled. We believe that the main reason for the fast clogging is related to the fact that these wells are planned only for monitoring purpose . As a consequence, the piezometers were not sufficiently developed. As for Pz101, the screens are totally clogged by bentonite and mud from the depth of 35 m to 53 m (Figure 2g). Below the depth of 53 m to the Pz101 bottom at 60 m, the screens are partially clogged (Figure 2h). The clogged intervals of the piezometers are represented on the technical logs (Figure 2b and c).

3. Experiment and methodology

3.1. Experimental set up

ADTS experiments were conducted in Pz101 and Pz51. A loop of BRUsens fiber-optic cable (SOLIFOS - Fiber Optic Systems AG, Switzerland) was lowered to their annular space. It contains two multi-mode fibers encased in a sealed stainless steel capillary and covered by wire rope and a PVC jacket (Figure 3a). Two electrical cables were connected to the steel armor of both fiber branches of the loop, to allow the injection of electricity from a power controller. These connections were further sealed by epoxy resin. The induced temperature variation was monitored with a Silixa XT DTS unit reporting temperature every 25 cm at a 2 min sampling interval in Pz51 and 1 min sampling interval in Pz101 (Figure 3b).

In order to ensure contact with the porous media, while deployed in the borehole, each branch of the FO cable was slightly stretched and attached outside the polyvinyl chloride (PVC) tube every 3 meters (Figure 3c). This installation was similar to a previous study in 25 m depth boreholes [del Val et al., 2021]. For both piezometers, 50 meters of FO cable of each side of the loop remained outside the borehole for connection to the DTS unit, and for calibration purposes. Once the whole equipment installed, the gravel pack was added down, which embedded the FO cable in the gravel and prevented any cable shaking.

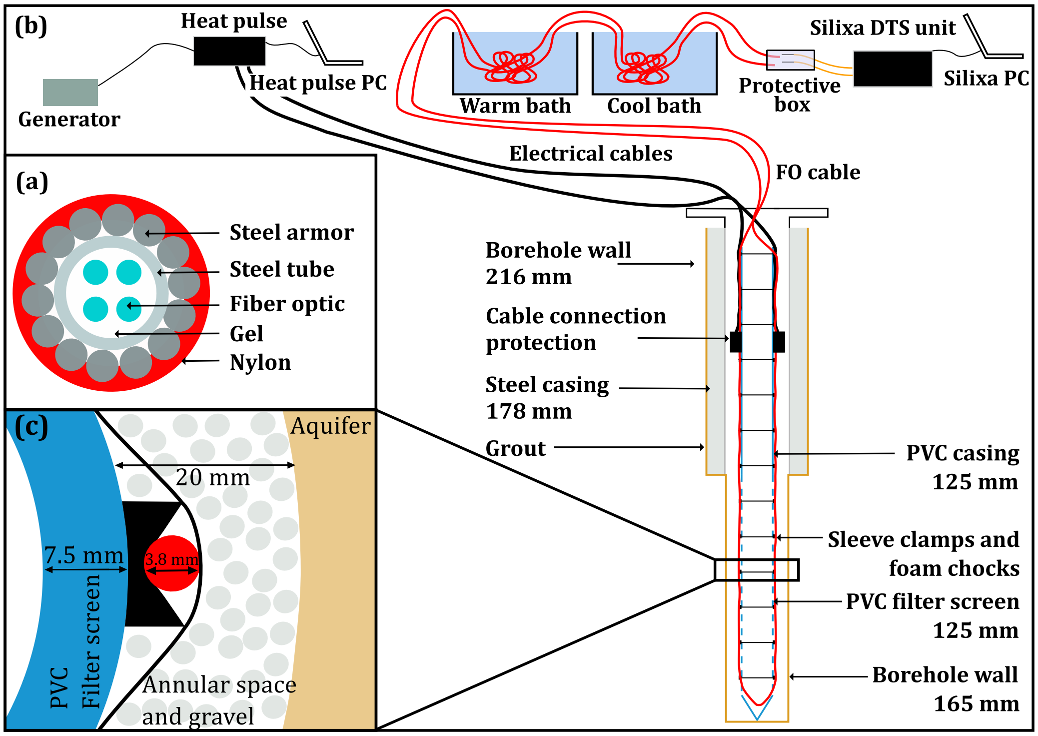

Figure 3: Device installation scheme : (a) transverse section of the FO cable, (b) scheme of experimental configuration with acquisition well and FO-DTS set up, (c) traverse borehole section representing fiber configuration in annular space

3.2. Temperature calibration process and DTS spatial resolution

During the experiment, 10 meters of each branch from sticking out cables were immersed into separate warm and cold calibration baths for temperature calibration purposes. In order to cover the full range of temperatures that could be expected to be measured along the fiber optic cable, the cold bath was filled with ice and the warm bath was equipped with a resistance to maintain water temperature at 31°C (Figure 3b). The temperature was recorded in each bath with a PT100 probe (0.1°C accuracy) and two RBR SoloT probes (0.002°C accuracy). The temperature in both baths was homogenized with small aquarium bubblers. The loop configuration of the fiber in the boreholes allowed to create a double-ended connection providing accurate temperature measurements under field conditions [van de Giesen et al., 2012]. The Python toolbox [des Tombe et al., 2020] was used to check the quality of the DTS measurement and indicated a good calibration of the temperature measured by the DTS device.

The DTS spatial resolution (S.R) during the experience was estimated from the classical 90% step change [Tyler et al., 2009] and the derivative method [Simon et al., 2020]. For Pz101, the S.R was estimated between 0.9 and 1.1 m. As the sampling time (S.T) was twice larger for Pz51 experiment, the S.R was better and range from 0.7 to 0.9 m. The S.R of these experiments were more precise than the 2–3 m S.R reported in the study of Tyler [Tyler et al., 2009] and slightly less precise than the 0.5–0.9 m S.R reported in the laboratory study of Simon [Simon et al., 2020].

3.3. Experiments proceedings

The experiment was ran under cross-borehole configuration. It is a common practice for integrated aquifer characterization. It is an efficient method to explain complex hydraulic behavior of aquifers and investigate preferential flow-path in heterogeneous contexts [Butler and Zhan, 2004, Le Borgne et al., 2006a,b, Audouin and Bodin, 2008, Brauchler et al., 2010, Lods et al., 2020, Aliouache et al., 2021]. This configuration is therefore of great interest to study thermal transfer by advection at the aquifer scale. The cross-borehole configuration was replicated into Pz101 and Pz51 to verify the reciprocity of the acquired data. The reciprocity can be used to interpret the dynamic of the aquifers and highlights continuity or not of the hydraulic system [Hariga et al., 2010, Delay et al., 2011, 2012, Marinoni et al., 2016, Sanchez-Vila et al., 2016].

The experiment started once the hydrodynamic pseudo-steady state was reached. The first stage consisted in heating the steel mantle of the fiber in the well Pz101 with a constant injection rate of power P trough electrical cables controlled by the Heat Pulse power controller. At the same time, the neighboring piezometer Pz51 was pumped at a constant rate Q varying in between 4.5 and 4.6 m^3/h depending on the experiment (Experiment 1 in Figure 4). The water level was monitored with vented Level Troll probes (In Situ) in both piezometers. The temperature evolution along the FO cable induced by the heat injection was monitored by the DTS device. At the end of the first stage, without stopping the heating of the fiber, the pumped water was injected in the monitoring well to monitor thermal signals induced by the injection (Experiment 2 in Figure 4). The injected water came from the aquifer under natural conditions, consequently it was colder than the water warmed by the fiber in the monitoring piezometer. Experiments 3 and 4 (Figure 4) correspond to ADTS experiment replicated in Pz51.

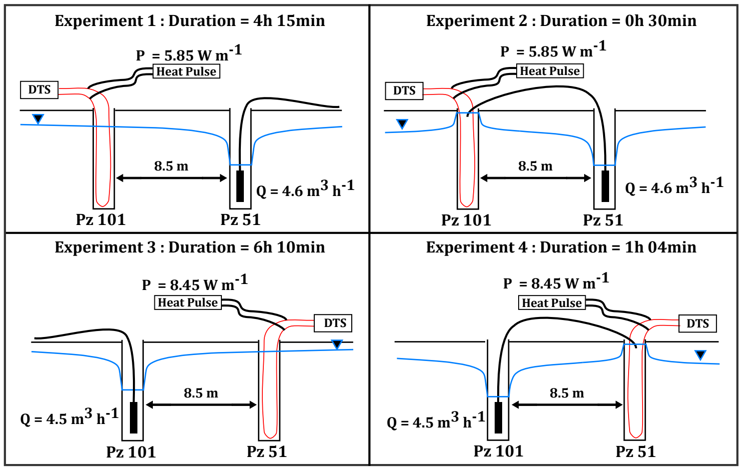

Figure 4: Scheme of the four experiment configurations with the indicated injected power by the heat pulse P and the pumping rate Q.

4. Experimental data analysis

Before the heating phase, the initial temperature distribution was recorded. It represented a C-shape with a minimum temperature of 15.4 °C between the length interval of 35–65 m depth (Figure 5a). Such a temperature profile is typical for subsurface temperature regime influenced by an increase in ground surface temperature caused by global warming and/or urbanization[Dědeček et al., 2012, Visser et al., 2015, Bayer et al., 2016]. Figure 5b represents transient temperature profiles along Pz51 (455 curves) acquired during the heating phase of the experiment.

As pointed out by the heat map, the U-shape of the cable provided two similar data sets at each sampling depth in Pz51. Data from Pz101 (423 curves, not displayed in Figure 5) are analyzed further in the manuscript. When the heating started (Experiment 1 and 3), there was a quick temperature increase along the cable, followed by a phase of slow change. As expected, differences of temperature elevation along the wells were observed due to thermal and hydrodynamic properties contrasts of aquifer layers [Simon et al., 2021, Zhang et al., 2020]. In some intervals, like 35 - 40 m depth the temperature reached a value of 25 °C, whereas at 45 m depth the temperature quickly stabilized around 18 °C. Such differences in thermal behavior along the well are analyzed in the following sections. During the water injection (Experiments 2 and 4) the temperature changes were less significant. Once the electrical power switched off, the temperature along the FO cable decreased drastically.

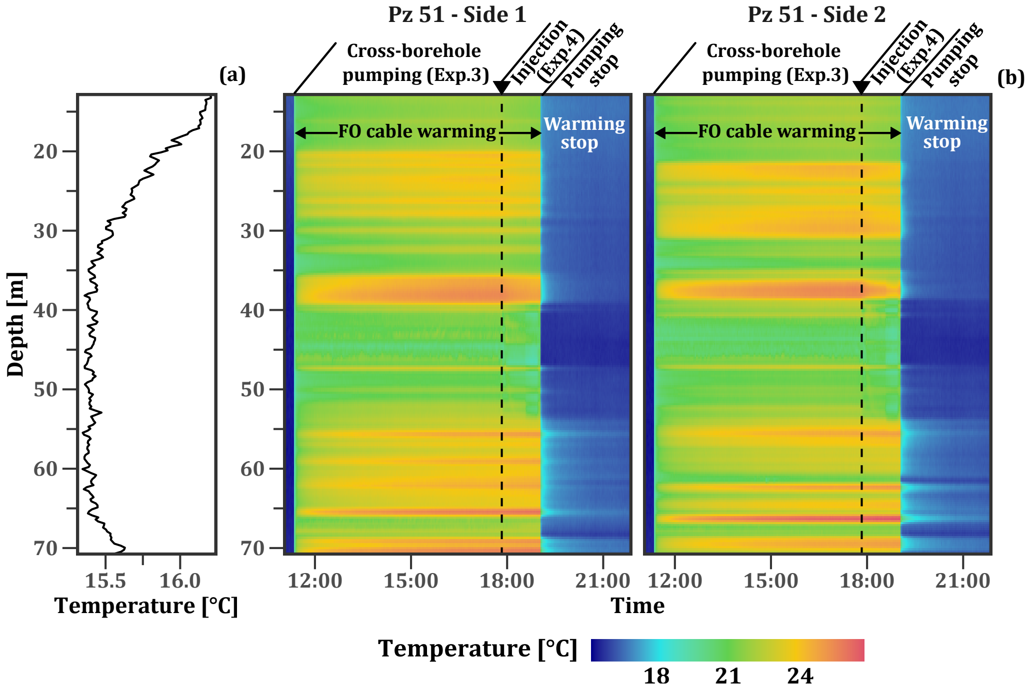

Figure 5: Temperature distribution along the FO cable in Pz51: (a) natural *in-situ* profile before the heating and (b) temperature variation with both time and depth along the two side of the FO loop. The temperatures measured at each side of the U cable are similar

4.1. Preferential water flux pathways during reinjection

The temperature anomalies measured during reinjection Experiments 2 and 4 informed about the preferential flow paths in front of the screens during injection. These anomalies were emphasized by the relative temperature anomaly ΔT_{inj} (Equation 1) induced by the injected water:

$$\Delta T_{inj} = T_t - T_{inj.start} \tag{1}$$

where $T_{inj.start}$ is the temperature profile just before the beginning of water injection, and T_t the temperature profile measured at the time t after the beginning of the injection. The evolution of ΔT_{inj} profiles revealed three different zones in both piezometers (Figure 6a and c).

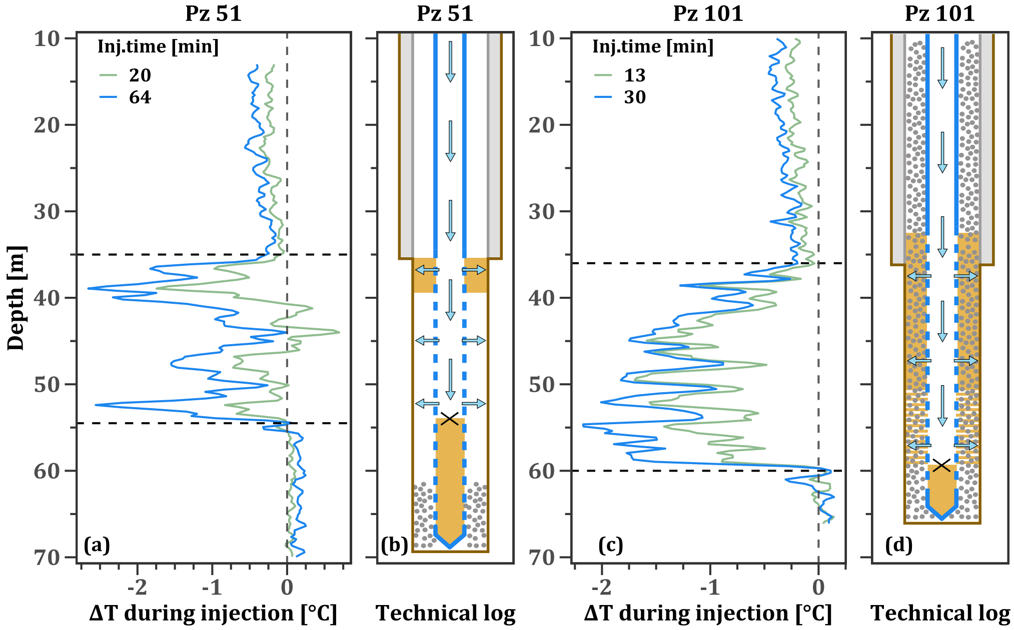

Figure 6: Experimental injection results : (a) and (c) relative temperature anomalyprofiles ΔT_{inj} at different times since the beginning of the injection;(b) and (d) technical log with identified clogged area from video inspection and flux pathway deduced from injection experiment represented by blue arrows

First, above the screens, i.e., at 35 m depth, in the grouted area, the injected water induced a slight temperature decrease less than 0.5 °C in both wells. This was related to conductive heat transfer due to colder water injection. For depths greater than 54.5 m in Pz51 and 60 m in Pz101, the water temperature continued to increase due to the cable heating. It indicated that, the injected water did not influence the evolution of borehole temperature. The latter means that the injected water did not infiltrate below these depths. Finally, in the middle parts of both wells, an overall significant temperature decrease induced by the local flow increase occurred in both piezometers. The water infiltration areas are identified on the technical log of both piezometers (Figure 6b and d). The thermal response was heterogeneous along the screens in both piezometers. For example, the layers at the depths of 39 m and 53 m in Pz51, or 54 m in Pz 101 were more sensitive to the cooling and reached a ΔT_{inj} of $-2.0\,^{\circ}\mathrm{C}$. Other layers, especially in Pz51 (41, 44 and 50 m), were barely affected by the cooling.

The short duration of the Experiments 2 and 4 (30 min and 64 min respectively) did not allow a quantitative interpretation of the temperature transients and only provided a qualitative overview about zones of enhanced groundwater flow.

4.2. Use of analytical solutions for parameter distribution estimation

4.2.1. General interpretation framework

ADTS data interpretation of Experiment 1 and Experiment 3 consisted on estimating vertically distributed parameters λ and q in the observation borehole. The parameters were calculated at each sampling depth. It was achieved through the assessment of experimental temperature evolution curves measured by the DTS device, following the theoretical approach developed by [Simon et al., 2021]. The interpretation framework was inspired from the one proposed by a free available Matlab Toolbox Simon and Bour [2022], and detailed further.

The two-dimensional heat transport in saturated porous media (Equation 2) involving conduction and advection processes is expressed as [Carslaw et al., 1959] :

$$\frac{\partial T}{\partial t} = D_t \left(\frac{\partial^2 T}{\partial x^2} + \frac{\partial^2 T}{\partial y^2} \right) - q \frac{\rho_w c_w}{\rho_b c_b} \frac{\partial T}{\partial x}, \tag{2}$$

where T is the temperature [K], x and y are the coordinates [m], q is the Darcy velocity [$\mathrm{m\,s^{-1}}$], $\rho_b c_b$ the volumetric heat capacity of the rock/fluid matrix [$\mathrm{J\,m^{-3}\,K^{-1}}$], $\rho_w c_w$ the volumetric heat capacity of the water [$\mathrm{J\,m^{-3}\,K^{-1}}$]. Ignoring thermal dispersion is a common practice for the interpretation of ADTS experiments [Bakker et al., 2015, Simon et al., 2021, del Val et al., 2021]. The consequences of this choice on the estimation of the parameters are discussed in subsection 5.2. Therefore, in Equation 2, only thermal diffusitivy D_t [$\mathrm{m^2\,s^{-1}}$] is involved. It depends on λ the bulk thermal conductivity [$\mathrm{W\,m^{-1}\,K^{-1}}$] and is expressed as :

$$D_t = \frac{\lambda}{\rho_b c_b}. \tag{3}$$

Considering whether or not natural flow in the aquifer occured, Equation 2 could be solved for a linear heating source involving the Instantaneous Line Source model (ILS) or Moving Instantaneous Line Source model (MILS) [Carslaw et al., 1959]. The ILS solution expressed as follows (Equation 4), considers no-flow within the aquifer and is the solution to Equation 2 without considering the second term:

$$\Delta T(r,t)_{ILS} = \frac{P}{4\pi\lambda}\left[E_i\left(\frac{-r^2}{4tD_t}\right)\right], \tag{4}$$

where ΔT is the temperature evolution, P [$\mathrm{W\,m^{-1}}$] is the constant heating power per unit length, $r^2 = x^2 + y^2$ is the distance from the heating source.

The MILS solution (Equation 5) is adapted from the ILS and considers uniform flow across the heat source to take into account heat transfer by advection. It is expressed as :

$$\Delta T(r,t)_{MILS} = \frac{P}{4\pi\lambda}\exp\left[\frac{qr}{2D_t}\frac{\rho_w c_w}{\rho c}\right]W(\alpha,\beta) \tag{5}$$

with $W(\alpha,\beta)$ the Hantush well function [Hantush, 1956]. λ and q are estimated from these two solutions.

The previous equations did not consider thermal effects induced by the heating of the cable itself and the borehole material configuration. Just after heat injection in the FO cable, the temperature increase was mainly associated, first, to the conductive skin effect in the FO cable components and secondly to the borehole material arrangement [del Val et al., 2021, Simon et al., 2021]. It generated a rapid increase of the temperature during the first time after heat injection. The effect of the cable was the same along the borehole. Nevertheless, the effect of the borehole material on the temperature increase could be different along the FO, depending on the cable

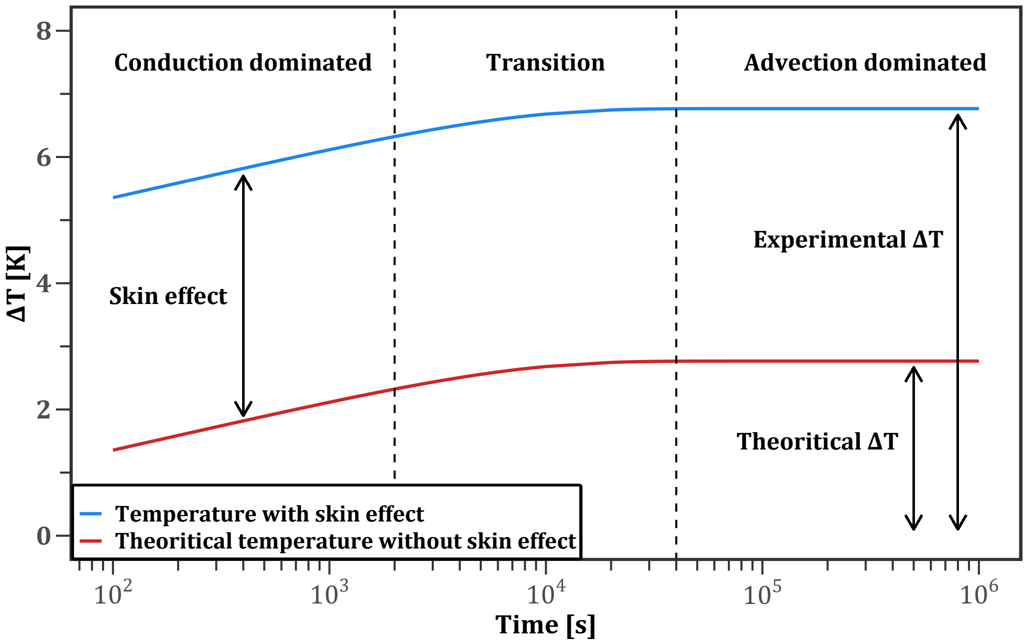

Figure 7: Theoretical temperature evolution in response to a heat pulse in saturated porous media with and without skin effect of the FO cable (adapted from [del Val et al., 2021]

position in the gravel pack and mud and its relative distance to the PVC tube. This aspect lead to a difference between the theoretical temperature calculated with ILS and MILS and the ΔT_{exp} measured by FO-DTS. This difference was taken into account in a ΔT_{FO} term (Figure 7). Thus, to model the temperature increase during the experiment, ΔT_{FO} was added to the ILS and MILS solutions. This was solved by trial/error adjustments between ILS model and experimental data.

4.2.2. Parameters quantification

The ILS and MILS solutions were adjusted on the experimental data to estimate the λ and q values associated with the temperature evolution

(Figure 8). The method consisted in reducing the Root Mean Square Error between the observed and modeled temperature using the Brent algorithm [Brent, 1974]. Four typical thermal behaviors were identified during the ADTS experiments, ranging from no-flow and low-flow towards medium-flow and high-flow.

For no-, low- and medium- Darcy velocity ($< 2.0 \times 10^{-5}\,\mathrm{m\,s^{-1}}$), the experimental points before 1000 seconds were assimilated to the skin effect. Thus, these points were excluded from λ fitting and estimation procedure (Figure 8 a-c). When only conductive heat transfer occurred, (i.e. no-flow) the temperature increased linearly along a log time scale during the whole experimental time (Figure 8a). In this case, the ILS solution was used to estimate λ. Advection transfer generated a transition phase until temperature stabilization (Figure 8b and c), and both analytical solutions were used to estimate λ and q.

High groundwater flux generated quick temperature stabilization. When the Darcy velocity was too high ($> 2.0\times10^{-5}\,\mathrm{m\,s^{-1}}$), the sampling time of the experiments was unsuited to visualize the linear part of the thermal evolution plot (an example is provided in Figure 8d). Consequently, thermal conductivity λ could not be estimated properly and was fixed at $2.8\,\mathrm{W\,m^{-1}\,K^{-1}}$. This value corresponds to an average value for limestone rocks [Dalla Santa et al., 2020]. Further discussion about the impact of λ values on the estimated q value is given in subsection 5.2.

The analytical models had a good fit to the field data, ,with the value of

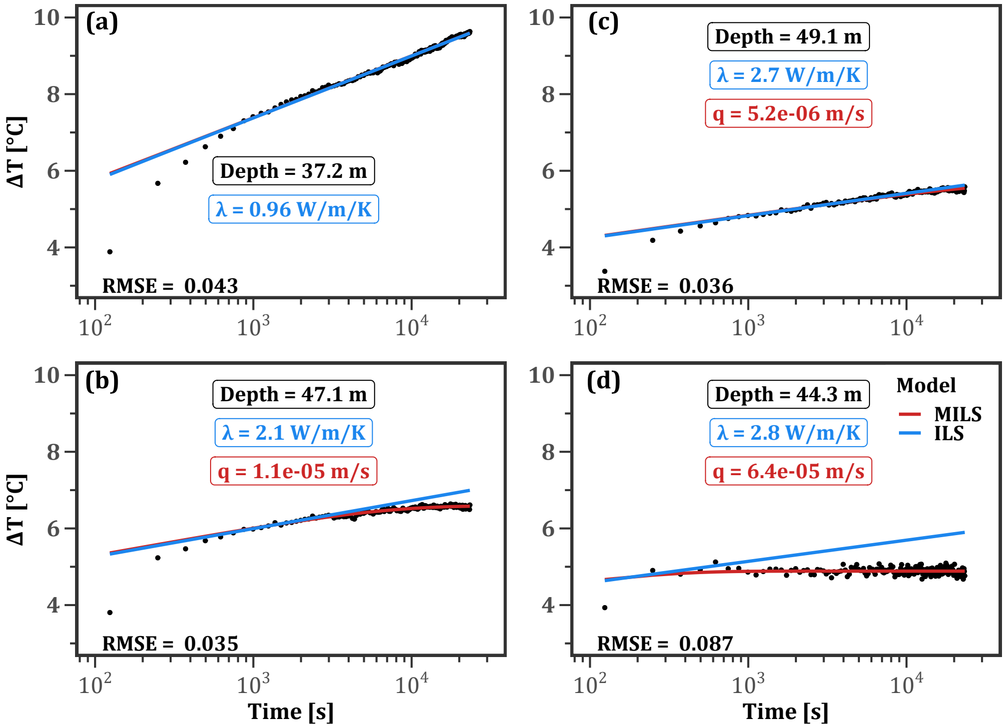

Figure 8: Determination of mean thermal conductivity λ and Darcy velocity q (piezometer Pz51) when, (a) only conduction occurs, (b) low flux is detected, (c) medium flux and (d) high flux occur with an early temperature stabilization due to higher groundwater flow.

the Root Mean Square Error (RMSE) generally remaining low, i.e. RMSE$<$ 0.1. The maximum value of 0.15 was calculated for the high Darcy velocity interval.

Low q values below 3.0x10^{-6} $\mathrm{m\,s^{-1}}$ should be considered cautiously. It was demonstrated that an experimental time of 24h with an error of ±0.05 °C on the field temperature measurement, lead to errors above 20% on q estimation [Simon et al., 2021]. This error grew exponentially with the decrease of estimated q.

4.2.3. Groundwater and thermal conductivity distribution

Vertical distribution of λ and q were computed for each sampling depth along the two branches of the U cable (Figure 9). In each piezometer, the 2 branches gave similar parameter estimations, suggesting the consistency of the data acquisition and its processing. The uncertain q values below $3.0 \times 10^{-6}\,\mathrm{m\,s^{-1}}$ were represented in a shaded area on the corresponding profiles (Figure 9a and c).

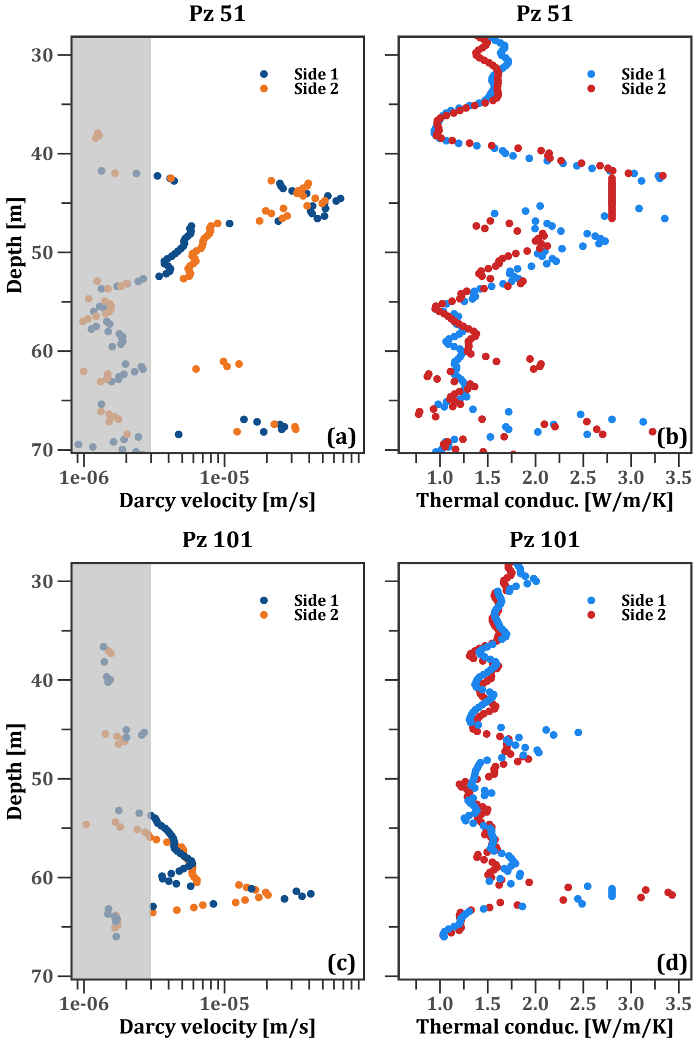

Figure 9: Parameter profiles estimated from FO-ADTS experiments in front of screened areas : (a and c) groundwater flux profiles, shaded areas correspond to estimated values with high uncertainty, (b and d) thermal conductivity profiles

Despite the short distance between Pz101 and Pz51 (8.5 m), the estimated q profiles showed major discrepancies in front of the borehole screens. These q profiles were not equally distributed along the flowing areas of both piezometers, highlighting a reciprocity gap. In Pz51, high Darcy velocities of $5.0 \times 10^{-5}\,\mathrm{m\,s^{-1}}$ were estimated in the intervals of 43–46 m and 67–68 m (Figure 9a). A lower peak of $1.0 \times 10^{-5}\,\mathrm{m\,s^{-1}}$ was detected in one branch at the depth of 62 m. From the depth of 46 m to 53 m, the q value decreased from $7.0 \times 10^{-6}\,\mathrm{m\,s^{-1}}$ to $4.0 \times 10^{-6}\,\mathrm{m\,s^{-1}}$. As for Pz101, the ADTS experiment allowed to estimate a high Darcy velocity superior of $2.0 \times 10^{-5}\,\mathrm{m\,s^{-1}}$ only in the thin layer at the depth of 62 m. A medium flow of an average of $5.0 \times 10^{-6}\,\mathrm{m\,s^{-1}}$ was estimated between the length interval 54–61 m (Figure 9c).

In front of the screens, the low λ values were always estimated in front of no- or low flux areas. In Pz51, a value close to $1.0\,\mathrm{W\,m^{-1}\,K^{-1}}$ was estimated in the length intervals 35–39 m and 54–67 m. On the contrary, high λ values were calculated where significant q values were calculated. This trend was also detected in Pz101. High λ values of $3.0\,\mathrm{W\,m^{-1}\,K^{-1}}$ were measured in front of the highest Darcy velocity area at the depth of 62 m, whereas the values fluctuated around $1.5\,\mathrm{W\,m^{-1}\,K^{-1}}$ in the rest of the piezometer.

5. Discussion

5.1. Consistency of the ADTS results in relation with available field data

The parameters profiles obtained from ADTS experiments were compared to available independent field data. The q profile in Pz51 emphasized the same high productive layer as the one detected in the GF1 flowmeter log at the depth of 44–46 m. The Darcy velocity reached a value of $5.0 \times 10^{-5}\,\mathrm{m\,s^{-1}}$

at this depth. Nevertheless, the flowmeter log achieved one year after borehole completion in Pz101 suggested a homogeneous flux distribution probably influenced by the clogging development along this borehole. But, the ADTS detected a medium Darcy velocity of $5.0 \times 10^{-6}\,\mathrm{m\,s^{-1}}$ where the screens are just partially clogged below the depth of 53 m.

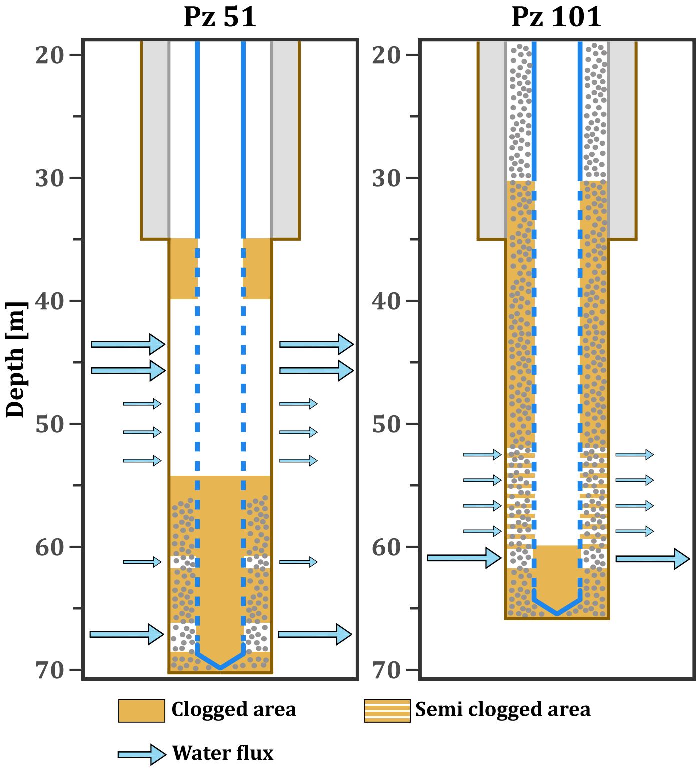

Figure 10: Interpretation scheme of boreholes clogging and flux location according to video inspection, parameters distribution and injection flow paths

In both piezometers, weak or zero Darcy velocity values were measured in front of clogged layers detected during video inspection (Figure 2f, g, and h). The λ values of these layers were always inferior to $1.5\,\mathrm{W\,m^{-1}\,K}$

(Figure 9b and d). It is typical for clogging materials like clay, bentonite and porous iron hydroxides [Dalla Santa et al., 2020, Cho et al., 2008, Tang et al., 2008, Gjengedal et al., 2020] and does not correspond to the typical values of the thermal conductivity of the limestone, i.e. $3.0\,\mathrm{W\,m^{-1}\,K}$. These observations highlight the potential of ADTS experiments to locate zones of borehole clogging. We believe that the main reason for the clogging is related to the fact that these wells were planned only for monitoring purpose, and, as a consequence, were not sufficiently developed after their completion. The clogged materials did not have the same position along both boreholes .It seems to be the main explanation for reciprocity gaps between parameters distribution in Pz51 and Pz101. The drill cuttings assessment revealed the same geology in both boreholes. But, a fracture or a more productive area might be intercepted in Pz51 and GF1 and not in Pz101 and could be the reason of a high flux in Pz51 and GF1, involving the dilution of the bentonite in Pz51 and not in Pz101.

The video camera showed bentonite and clay at the bottom of both piezometers. The position of the plugs, at the depth of 54.5 m in Pz51 and 60 m in Pz101, corresponded exactly to the limits highlighted by Experiment 2 and Experiment 4 (Figure 6). It confirmed that during injection, the water did not flow in the lower part of the piezometers. Nevertheless, during Experience 1 and Experience 3, some fluxes were detected below the well bottoms, at the depths of 62 m in Pz101 and 62 m and 68 m in Pz51 (Figure 10). It may point out that at these depths, the boreholes were clogged but the deposits were not completely compacted/encrusted into the annular space. High thermal conductivity values ($> 3.0\,\mathrm{W\,m^{-1}\,K^{-1}}$) may confirm a likely dilution of the mud in these intervals.

5.2. Uncertainty and resolution of parameters calculation

In highly productive layers, the groundwater flow generated a fast temperature stabilization. In this context, ADTS experiments with a sampling time of more than 1 minute are unsuited to visualize the linear part of the ΔT_{exp} plot before the temperature stabilization (Figure 8d). Consequently, it is not possible to accurately estimate the thermal conductivity λ. Consequently, values of thermal conductivity consistent with the properties of the porous material [Dalla Santa et al., 2020] encountered in the borehole must be chosen as the default value. However, in high productive context, it is possible to demonstrate the low impact of λ on the estimated Darcy velocity (Figure 11). A sampling time of a few seconds would be necessary to visualize the conductive phase in this context. Nevertheless, a short sampling time produce noisier data which can also lead to high uncertainty [des Tombe et al., 2020].

As mentioned in section 4.2.1, the analytical model used in this study ignored thermal dispersion. By doing this, the thermal diffusivity is overestimated. It could be another source of error that could lead to underestimating q, especially in high-flow areas. It was demonstrated that an estimated q of $5.0 \times 10^{-6}\,\mathrm{m\,s^{-1}}$ without considering the thermal dispersion

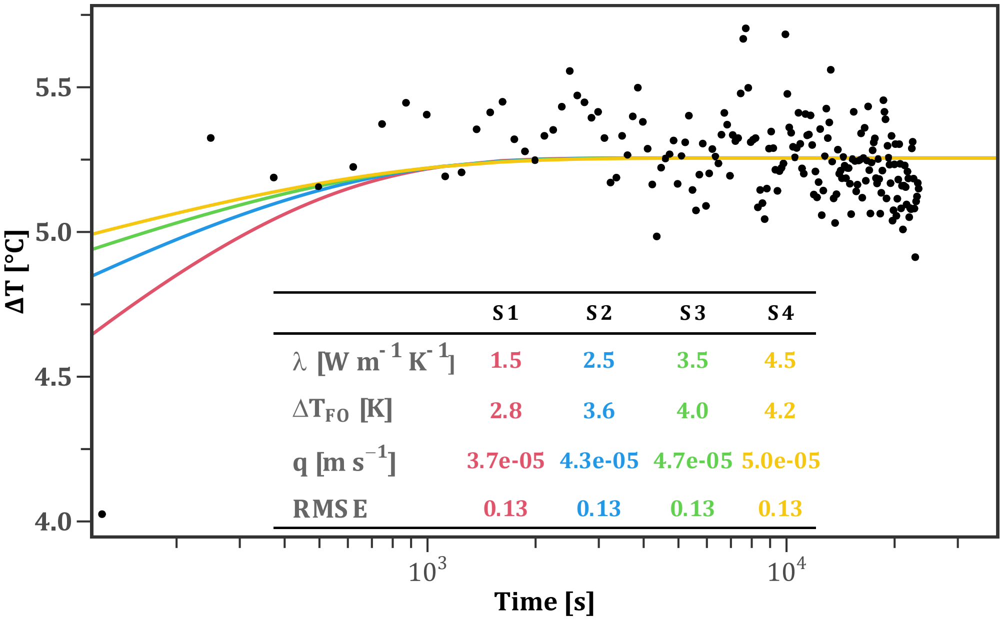

	S1	S2	S3	S4
λ [W m^{-1} K^{-1}]	1.5	2.5	3.5	4.5
ΔT_{FO} [K]	2.8	3.6	4.0	4.2
q [m s^{-1}]	3.7e-05	4.3e-05	4.7e-05	5.0e-05
RMSE	0.13	0.13	0.13	0.13

Figure 11: Analytical solutions generated from the framework to reproduce experimental temperature evolution at 45.2m in Pz51 with a large scale of λ from 1.5 to 4.5 $\mathrm{W\,m^{-1}\,K^{-1}}$

will yield a q of $9.0 \times 10^{-6}\,\mathrm{m\,s^{-1}}$ if the longitudinal dispersivity is set at 0.1 m [des Tombe et al., 2019]. Nevertheless, in our experiment, the effect of thermal dispersion should be very small, if not negligible, since here, we use the same cable as a heat source and for measuring temperature.

Moreover, the vertical resolution of the DTS is a limit to measure temperature variations induced by layers with a thickness ranging this resolution. Even if a thin layer is detected by the FO DTS experiment, the measured temperature in front of this layer is a result of the surrounding conditions leading to uncertainty in parameter estimation [des Tombe et al., 2019, Simon et al., 2020].

Finally, parameters estimation, especially λ estimation, is influenced by the test configuration. The resolved parameters are unlikely to provide the true aquifer properties since the FO cable is located in the borehole annular space, close to the PVC tube, surrounded by the gravel and clogging material. Despite these uncertainties, one should rather focus on relative parameter variation to identify clogging locations and productive layers along the borehole.

5.3. Advantages and limits of the proposed ADTS experiments

5.3.1. Comparison with common field surveys

These experiments demonstrated that ADTS could provide in short time information regarding two crucial concerns for ATES operation: (i) the method provides important insights regarding the aquifer heterogeneity in thermal and hydrodynamic properties and (ii) it enables the detection of clogging locations in the borehole. ADTS experiment presents the advantage to estimate a distribution of parameters while pumping tests and TRT give an average value of hydrodynamics and thermal properties. Moreover, these surveys require much longer time of data collection (i.e., at least 48h versus 4-6 h required for the completion of ADTS tests). However, TRT and pumping tests are very simple to deploy, and their well-known and relatively quick interpretation can give a first overview of the global aquifer dynamics.

Unlike ADTS, flowmeter tests are not designed to provide information about conductive heat transfers which could be of great interest in geothermal projects. Nevertheless, the single-hole flowmeter is a common survey that can be achieved in a shorter time than ADTS, after a borehole completion. It has also the advantage of a more simple setup than the ADTS one. It provides a local vertical distribution of the fluxes at the logging well, and is used to estimate permeability variations along the aquifer [Molz et al., 1989, 1994, Paillet, 1998]. The application of the flowmeter test in cross-borehole configuration proved to be also an efficient methodology to have a better characterization of aquifer dynamics at a large scale. It allows highlighting connectivity of preferential groundwater flow paths [Le Borgne et al., 2006a,b, Audouin and Bodin, 2008].

The ADTS experiments give thermal conductivity only in the vicinity of the monitoring well. To characterize aquifer heterogeneity and thermal diffusivity on large scales, heat tracer tests with multiple monitoring well may be more powerful experimental field test [Klepikova et al., 2016]. It provides additional information compared to solute tracer tests, since the thermal diffusivity is higher than the solute dispersion [Irvine et al., 2015, La Bernardie et al., 2018]. Consequently, heat tracer tests are more suited for geothermal sites. However, due to the ability of heat to propagate through solids by diffusion, completion of heat tracer tests may take much longer time compared to solute tracer tests (days vs hours).[Irvine et al., 2015, La Bernardie et al., 2018]. It can also be difficult to realize and interpret compared to ADTS experiments.

.

Recent studies [Gjengedal et al., 2020, 2021] based on short step-test combined with temperature and hydraulic performance monitoring, first demonstrated a new technique enabling the detection of clogging and its further evolution characterization in geothermal systems. While this method allows the detection of clogging in the entire system, it does not precise the clogging location in the boreholes. The new characteristic of our ADTS interpretation is to image clogging distribution in the monitoring well. Therefore, this new strategy and the one proposed by Gjengedal et al. [2020] could complement each other. Once deployed in the borehole, and all cable connections realized, ADTS technology could be used as a permanent *in-situ* device. It presents a certain advantage as it can collect a large amount of data without opening the borehole and removing the submersible pump. The aim would be to monitor clogging evolution and aquifer properties changes over time and to plan and adapt maintenance works before major deterioration of the wells. This aspect would be time and financial saving compared to diagnostic well works, or video camera inspections to visualize clogging development. It is also an advantage to have a permanent fiber in the borehole. It allows to warm the cable and collect the data with the DTS unit without deploying the fiber in the borehole before each experiment like the methodology proposed by Maldaner et al. [2019].

5.3.2. Potential limits of cross-borehole ADTS experiments in a geothermal operational context

Our experiments were achieved in wells made of PVC tubes and screens. This material has a low thermal conductivity of $0.2\,\mathrm{W\,m^{-1}\,K^{-1}}$. It gives a limited impact on the temperature evolution generated by the warming of the fiber. This impact was included in the skin effect during our interpretation process. Nevertheless, a lot of wells are made of steel or stainless steel. Because of the high thermal conductivity of this material (15-30 $\mathrm{W\,m^{-1}\,K^{-1}}$), the energy demand may be significant to create a temperature increase detectable by the DTS device. A numerical model taking into account a well equipped with steel material would be necessary to inspect the feasibility of ADTS experiment in this configuration.

While on the ENSEGID site, the exploited aquifer is found at a shallow depth (35-65 m), in other sites, the geothermal target may be deeper. The longer cable length required for deeper applications will generate an additional economic cost, and the deployment of the technology in the borehole will be more time-consuming. Moreover, longer heated section of the cable will require more power injection to reach similar temperature variations. In this context, it is a major concern to provide suitable devices able to inject safely more electrical power.

Finally, the ENSEGID site is equipped with several wells close to each other, thus offering a good opportunity to perform ADTS experiments in cross-borehole configuration. Monitoring and pumping boreholes are only separated by a distance of 8.5 m and a flowrate inferior to $5.0\,\mathrm{m^3\,h^{-1}}$ was enough to induce groundwater flux measurable by the ADTS experiment. Nevertheless, on geothermal sites just equipped with a warm and a cold well, the high distance (generally more than 100 meters) between the wells to avoid thermal breakthrough, may be a limit to perform cross-borehole ADTS experiments. Depending on the hydrogeological context and the capacity of the installed submersible pump, the groundwater velocity at the monitoring well may not be detectable by the presented ADTS experiment configuration and interpretation scheme. In this case, a single-hole ADTS configuration, like the one proposed by Read et al. [2014], may be more suited.

6. Conclusion

This study demonstrated the potential of ADTS experiments to collect and interpret a large amount of data by placing a FO between the borehole screens and the porous media. Our study allowed to characterize simultaneously the distribution of thermal conductivity and Darcy velocity in a short time (4-6 hours per experiment), and to get useful insights about the water injection pathways in boreholes. Moreover, the data provided information concerning the position of the clogging development along the screens.

In the future, it would be certainly of interest to test ADTS experiments on a new operational geothermal site. The aim would be to determine initial parameters profiles before the beginning of ATES operation in the production/injection wells, and then, monitor their evolution during a long-term operation to have an overview on the wells performance behavior.

References

Mohammed Aliouache, Xiaoguang Wang, Pierre Fischer, Gerard Massonnat, and Herve Jourde. An inverse approach integrating flowmeter and pumping test data for three-dimensional aquifer characterization. Journal of Hydrology, 603, 2021. ISSN 00221694. doi: 10.1016/j.jhydrol.2021.126939.

Olivier Audouin and Jacques Bodin. Cross-borehole slug test analysis in a fractured limestone aquifer. Journal of Hydrology, 348(3-4):510–523, 2008. ISSN 00221694. doi: 10.1016/j.jhydrol.2007.10.021. URL `https://linkinghub.elsevier.com/retrieve/pii/S0022169407006129`.

G. Bakema. Well and Borehole Failures and Solutions in Underground Thermal Energy Storage. 2001. doi: 10.13140/RG.2.2.10214.98885.

Mark Bakker, Ruben Caljé, Frans Schaars, Kees-Jan van der Made, and Sander de Haas. An active heat tracer experiment to determine groundwater velocities using fiber optic cables installed with direct push equipment. Water Resour. Res., 51:2760–2772, 2015. ISSN 0043-1397, 1944-7973. doi: 10.1002/2014WR016632.

Peter Bayer, Jaime A. Rivera, Daniel Schweizer, Ulrich Schärli, Philipp Blum, and Ladislaus Rybach. Extracting past atmospheric warming and urban heating effects from borehole temperature profiles. Geothermics, 64:289–299, 2016. ISSN 03756505. doi: 10.1016/j.geothermics.2016.06.011.

Richard A. Beier, Marvin D. Smith, and Jeffrey D. Spitler. Reference data sets for vertical borehole ground heat exchanger models and thermal response test analysis. Geothermics, 40:79–85, 2011. ISSN 03756505. doi: 10.1016/j.geothermics.2010.12.007.

V. F. Bense, T. Read, O. Bour, T. Le Borgne, T. Coleman, S. Krause, A. Chalari, M. Mondanos, F. Ciocca, and J. S. Selker. Distributed Temperature Sensing as a downhole tool in hydrogeology: SUBSURFACE DTS. Water Resour. Res., 52(12):9259–9273, 2016. ISSN 00431397. doi: 10.1002/2016WR018869.

M. Bloemendal and T. Olsthoorn. ATES systems in aquifers with high ambient groundwater flow velocity. Geothermics, 75:81–92, 2018. ISSN 03756505. doi: 10.1016/j.geothermics.2018.04.005.

Martin Bloemendal and Niels Hartog. Analysis of the impact of storage conditions on the thermal recovery efficiency of low-temperature ATES systems. Geothermics, 71:306–319, 2018. ISSN 03756505. doi: 10.1016/j.geothermics.2017.10.009.

J. Bodin, F. Delay, and G. de Marsily. Solute transport in a single fracture with negligible matrix permeability: 2. mathematical formalism. Hydrogeology Journal, 11:434–454, 2003. ISSN 1431-2174, 1435-0157. doi: 10.1007/s10040-003-0269-1.

R. Brauchler, R. Hu, T. Vogt, D. Al-Halbouni, T. Heinrichs, T. Ptak, and

M. Sauter. Cross-well slug interference tests: An effective characterization method for resolving aquifer heterogeneity. Journal of Hydrology, 384(1-2): 33–45, 2010. ISSN 00221694. doi: 10.1016/j.jhydrol.2010.01.004.

Richard P. Brent. Algorithms for Minimization Without Derivatives. Mathematics of Computation, 28(127):865, 1974. ISSN 00255718. doi: 10.2307/2005713.

D. W. Bridger and D. M. Allen. Influence of geologic layering on heat transport and storage in an aquifer thermal energy storage system. Hydrogeol J, 22:233–250, 2014. ISSN 1431-2174, 1435-0157. doi: 10.1007/s10040-013-1049-1.

James J. Butler and Xiaoyong Zhan. Hydraulic tests in highly permeable aquifers. Water Resour. Res., 40(12), 2004. ISSN 00431397. doi: 10.1029/2003WR002998.

Horatio Scott Carslaw, John Conrad Jaeger, and Jaeger Jaeger, John Conrad. Conduction of Heat in Solids. Clarendon Press, 1959. ISBN 978-0-19-853368-9.

W. Cho, Jae-Owan Lee, and Sangki Kwon. Thermal Conductivity of Compacted Bentonite and Bentonite-Sand Mixture. Journal of the Korean Radioactive Waste Society, 2008. URL `https://www.semanticscholar.org/paper/`

`Thermal-Conductivity-of-Compacted-Bentonite-and-Cho-Lee/3dcdbbee80e6104837c4961adfaf93f744b771b8`.

Giorgia Dalla Santa, Antonio Galgaro, Raffaele Sassi, Matteo Cultrera, Paolo Scotton, Johannes Mueller, David Bertermann, Dimitrios Mendrinos, Riccardo Pasquali, Rodolfo Perego, Sebastian Pera, Eloisa Di Sipio, Giorgio Cassiani, Michele De Carli, and Adriana Bernardi. An updated ground thermal properties database for GSHP applications. Geothermics, 85: 101758, 2020. ISSN 03756505. doi: 10.1016/j.geothermics.2019.101758.

Laura del Val, Jesús Carrera, María Pool, Lurdes Martínez, Carlos Casanovas, Olivier Bour, and Albert Folch. Heat Dissipation Test With Fiber-Optic Distributed Temperature Sensing to Estimate Groundwater Flux. Water Res, 57, 2021. ISSN 0043-1397, 1944-7973. doi: 10.1029/2020WR027228.

Frederick Delay, Philippe Ackerer, and Alberto Guadagnini. Theoretical analysis and field evidence of reciprocity gaps during interference pumping tests. Advances in Water Resources, 34:592–606, 2011. ISSN 03091708. doi: 10.1016/j.advwatres.2011.02.006.

Frederick Delay, Philippe Ackerer, Benjamin Belfort, and Alberto Guadagnini. On the emergence of reciprocity gaps during interference pumping tests in unconfined aquifers. Advances in Water Resources, 46: 11–19, 2012. ISSN 03091708. doi: 10.1016/j.advwatres.2012.06.002.

Bas F. des Tombe, Mark Bakker, Frank Smits, Frans Schaars, and Kees-Jan Made. Estimation of the Variation in Specific Discharge Over Large Depth Using Distributed Temperature Sensing (DTS) Measurements of the Heat Pulse Response. Water Resour. Res., 55:811–826, 2019. ISSN 0043-1397, 1944-7973. doi: 10.1029/2018WR024171.

Bas.F des Tombe, Bart Schilperoort, and Mark Bakker. Estimation of Temperature and Associated Uncertainty from Fiber-Optic Raman-Spectrum Distributed Temperature Sensing. Sensors, 20:2235, 2020. ISSN 1424-8220. doi: 10.3390/s20082235.

Jierui Dong, Xuquan Li, Bo Han, Ran Tian, and Huili Yu. A regional study of in-situ thermal conductivity of soil based on artificial neural network model. Energy and Buildings, 257:111785, 2022. ISSN 03787788. doi: 10.1016/j.enbuild.2021.111785.

Petr Dědeček, Jan Šafanda, and Dušan Rajver. Detection and quantification of local anthropogenic and regional climatic transient signals in temperature logs from Czechia and Slovenia. Climatic Change, 113(3-4):787–801, 2012. ISSN 0165-0009, 1573-1480. doi: 10.1007/s10584-011-0373-5.

Grant Ferguson. Heterogeneity and Thermal Modeling of Ground Water. Ground Water, 45:485–490, 2007. ISSN 0017-467X, 1745-6584. doi: 10.1111/j.1745-6584.2007.00323.x.

P. Fleuchaus, B. Godschalk, I. Stober, and P. Blum. Worldwide application of aquifer thermal energy storage – A review. Renewable and Sustainable Energy Reviews, 94:861–876, 2018. ISSN 1364-0321. doi: 10.1016/j.rser.2018.06.057.

B. M. Freifeld, S. Finsterle, T. C. Onstott, P. Toole, and L. M. Pratt. Ground surface temperature reconstructions: Using in situ estimates for thermal conductivity acquired with a fiber-optic distributed thermal perturbation sensor. Geophys. Res. Lett., 35(14):L14309, 2008. ISSN 0094-8276. doi: 10.1029/2008GL034762.

Sayantan Ganguly and M.S. Mohan Kumar. Analytical solutions for movement of cold water thermal front in a heterogeneous geothermal reservoir. Applied Mathematical Modelling, 38:451–463, 2014. ISSN 0307904X. doi: 10.1016/j.apm.2013.06.031.

Liuhua Gao, Jun Zhao, Qingsong An, Junyao Wang, and Xueling Liu. A review on system performance studies of aquifer thermal energy storage. Energy Procedia, 142:3537–3545, 2017. ISSN 18766102. doi: 10.1016/j.egypro.2017.12.242.

H Ghaebi, M N Bahadori, and M H Saidi. Economic and environmental evaluation of different operation alternatives to aquifer thermal energy storage in Tehran, Iran. Scientia Iranica, page 14, 2017.

S. Gjengedal, L.A. Stenvik, R.K. Ramstad, Jan I. Ulfsnes, Bernt O. Hilmo, and Bjørn S. Frengstad. Online remote-controlled and cost-effective fouling and clogging surveillance of a groundwater heat pump system: A case study from Lena Terrace in Melhus, Norway. Bull Eng Geol Environ, 80:1063–1072, 2021. ISSN 1435-9529, 1435-9537. doi: 10.1007/s10064-020-01963-z.

Sondre Gjengedal, Randi K. Ramstad, Bernt O. Hilmo, and Bjørn S. Frengstad. Fouling and clogging surveillance in open loop GSHP systems: A systematic procedure for fouling and clogging detection in the whole groundwater circuit. Bull Eng Geol Environ, 79:69–82, 2020. ISSN 1435-9529, 1435-9537. doi: 10.1007/s10064-019-01556-5.

Petri Hakala, Sami Vallin, Teppo Arola, and Ilkka Martinkauppi. Novel use of the enhanced thermal response test in crystalline bedrock. Renewable Energy, 182:467–482, 2022. ISSN 09601481. doi: 10.1016/j.renene.2021.10.020.

Madih Salih Hantush. Analysis of data from pumping tests in leaky aquifers. Trans. AGU, 37:702, 1956. ISSN 0002-8606. doi: 10.1029/TR037i006p00702. URL `http://doi.wiley.com/10.1029/TR037i006p00702`.

Nejla T. Hariga, Amel Ben Abda, Rachida Bouhlila, and Jean-Raynald de Dreuzy. Definition and interests of reciprocity and reciprocity gap principles for groundwater flow problems. Advances in Water Resources, 33:899–904, 2010. ISSN 03091708. doi: 10.1016/j.advwatres.2010.04.015.

Heiko Huber and Ulvi Arslan. Geothermal Field Tests with Forced Groundwater Flow. page 5, Stanford University, Stanford, California, 2012.

E. Hurtig, S. Groswig, and K. Kühn. Fibre optic temperature sensing: application for subsurface and ground temperature measurements. Tectonophysics, 257:101–109, 1996. ISSN 00401951. doi: 10.1016/0040-1951(95)00124-7.

Dylan J. Irvine, Craig T. Simmons, Adrian D. Werner, and Thomas Graf. Heat and Solute Tracers: How Do They Compare in Heterogeneous Aquifers? Groundwater, 53:10–20, 2015. ISSN 0017467X. doi: 10.1111/gwat.12146.

Maria Klepikova, Samuel Wildemeersch, Thomas Hermans, Pierre Jamin, Philippe Orban, Frédéric Nguyen, Serge Brouyère, and Alain Dassargues. Heat tracer test in an alluvial aquifer: Field experiment and inverse modelling. Journal of Hydrology, 540:812–823, 2016. ISSN 00221694. doi: 10.1016/j.jhydrol.2016.06.066.

Maria Klepikova, Bernard Brixel, and Delphine Roubinet. Analysis of thermal dilution experiments with distributed temperature sensing for fractured rock characterization. Journal of Hydrology, 610:127874, 2022. ISSN 0022-1694. doi: https://doi.org/10.1016/j.jhydrol.2022.127874.

G. P. Kruseman and N. A. de Ridder. Analysis and evaluation of pumping test data. ILRI publication. International Institute for Land Reclamation and Improvement, Wageningen, 2. ed. (compl. rev.), repr edition, 1994. ISBN 978-90-70754-20-4. OCLC: 258203525.

J. La Bernardie, O. Bour, T. Le Borgne, N. Guihéneuf, E. Chatton, T. Labasque, H. Le Lay, and M.-F. Gerard. Thermal Attenuation and Lag Time in Fractured Rock: Theory and Field Measurements From Joint Heat and Solute Tracer Tests. Water Resour. Res., 54, 2018. ISSN 0043-1397, 1944-7973. doi: 10.1029/2018WR023199.

C. Labat, F. Larroque, B. de Grissac, A. Dupuy, M. Saltel, and P. Bourbon. Influence of an anticline structure on hydrogeological functioning and aquifer interactions in a multilayered aquifer system: the case of Villagrains-Landiras anticline (Gironde, France). Hydrogeol J, 29:1711–1732, 2021. ISSN 1431-2174, 1435-0157. doi: 10.1007/s10040-021-02333-z.

F. Larroque, O. Cabaret, O. Atteia, A. Dupuy, and M. Franceschi. Vertical heterogeneities of hydraulic aquitard parameters: preliminary results from laboratory and *in situ* monitoring. Hydrological Sciences Journal, 58: 912–929, 2013. ISSN 0262-6667, 2150-3435. doi: 10.1080/02626667.2013.783215.

T. Le Borgne, O. Bour, F.L. Paillet, and J.-P. Caudal. Assessment of preferential flow path connectivity and hydraulic properties at single-borehole and cross-borehole scales in a fractured aquifer. Journal of Hydrology, 328: 347–359, 2006a. ISSN 00221694. doi: 10.1016/j.jhydrol.2005.12.029.

Tanguy Le Borgne, Frederick Paillet, Olivier Bour, and Jean-Pierre Caudal. Cross-Borehole Flowmeter Tests for Transient Heads in Heterogeneous Aquifers. Ground Water, 44:444–452, 2006b. ISSN 0017-467X, 1745-6584. doi: 10.1111/j.1745-6584.2005.00150.x.

Gérard Lods, Delphine Roubinet, Jürg M. Matter, Richard Leprovost, and Philippe Gouze. Groundwater flow characterization of an ophiolitic hard-rock aquifer from cross-borehole multi-level hydraulic experiments. Journal of Hydrology, 589, 2020. ISSN 00221694. doi: 10.1016/j.jhydrol.2020.125152.

C. H. Maldaner, J. D. Munn, T. I. Coleman, J. W. Molson, and B. L. Parker. Groundwater Flow Quantification in Fractured Rock Boreholes Using Active Distributed Temperature Sensing Under Natural Gradient Conditions. Water Resour. Res., 55:3285–3306, 2019. ISSN 0043-1397, 1944-7973. doi: 10.1029/2018WR024319.

Marianna Marinoni, Frederick Delay, Philippe Ackerer, Monica Riva, and Alberto Guadagnini. Identification of groundwater flow parameters using reciprocal data from hydraulic interference tests. Journal of Hydrology, 539:88–101, 2016. ISSN 00221694. doi: 10.1016/j.jhydrol.2016.05.019.

F.J. Molz, G.K. Boman, S.C. Young, and W.R. Waldrop. Borehole flowmeters: field application and data analysis. Journal of Hydrology, 163(3-4): 347–371, 1994. ISSN 00221694. doi: 10.1016/0022-1694(94)90148-1.

Fred J. Molz, Roger H. Morin, Alfred E. Hess, Joel G. Melville, and Oktay Güven. The Impeller Meter for measuring aquifer permeability variations: Evaluation and comparison with other tests. Water Resour. Res., 25:1677–1683, 1989. ISSN 00431397. doi: 10.1029/WR025i007p01677.

Van Tam Nguyen, Thomas Graf, and Carlos R. Guevara Morel. Free thermal convection in heterogeneous porous media. Geothermics, 64:152–162, 2016. ISSN 03756505. doi: 10.1016/j.geothermics.2016.05.006.

F. L. Paillet. Flow modeling and permeability estimation using borehole flow logs in heterogeneous fractured formations. Water Resour. Res., 34: 997–1010, 1998. ISSN 00431397. doi: 10.1029/98WR00268.

M. Possemiers, M. Huysmans, and O. Batelaan. Application of multiple-point geostatistics to simulate the effect of small-scale aquifer heterogeneity on the efficiency of aquifer thermal energy storage. Hydrogeology Journal, 23, 2015. doi: 10.1007/s10040-015-1244-3.

T. Read, O. Bour, J. S. Selker, V. F. Bense, T. Le Borgne, R. Hochreutener, and N. Lavenant. Active-distributed temperature sensing to continuously quantify vertical flow in boreholes. Water Resour. Res., 50:3706–3713, 2014. ISSN 00431397. doi: 10.1002/2014WR015273.

Delphine Roubinet, James Irving, and Frederick D. Day-Lewis. Development of a new semi-analytical model for cross-borehole flow experiments in fractured media. Advances in Water Resources, 76:97–108, 2015. ISSN 03091708. doi: 10.1016/j.advwatres.2014.12.002.

X. Sanchez-Vila, P. Ackerer, F. Delay, and A. Guadagnini. Characterization of reciprocity gaps from interference tests in fractured media through a dual porosity model. Water Resour. Res., 52:1696–1704, 2016. ISSN 00431397. doi: 10.1002/2015WR018171.

S. Schüppler, P. Fleuchaus, and Philipp Blum. Techno-economic and environmental analysis of an Aquifer Thermal Energy Storage (ATES) in Germany. Geotherm Energy, 7:11, 2019. ISSN 2195-9706. doi: 10.1186/s40517-019-0127-6.

Frank Selker and John Selker. Investigating Water Movement Within and Near Wells Using Active Point Heating and Fiber Optic Distributed Temperature Sensing. Sensors, 18, 2018. ISSN 1424-8220. doi: 10.3390/s18041023.

Mostafa H. Sharqawy, Hassan M. Badr, and Esmail M. Mokheimer. Investigation of buoyancy effects on heat transfer between a vertical borehole heat exchanger and the ground. Geothermics, 48:52–59, 2013. ISSN 03756505. doi: 10.1016/j.geothermics.2013.04.003.

N. Simon and O. Bour. An ADTS Toolbox for Automatically Interpreting Active Distributed Temperature Sensing Measurements. Groundwater, page gwat.13172, January 2022. ISSN 0017-467X, 1745-6584. doi: 10.1111/gwat.13172.

N. Simon, O. Bour, N. Lavenant, G. Porel, B. Nauleau, B. Pouladi, L. Longuevergne, and A. Crave. Numerical and Experimental Validation of the Applicability of Active-DTS Experiments to Estimate Thermal Conductivity and Groundwater Flux in Porous Media. Water Res, 57, 2021. ISSN 0043-1397, 1944-7973. doi: 10.1029/2020WR028078.

Nataline Simon, Olivier Bour, Nicolas Lavenant, Gilles Porel, Benoît Nauleau, Behzad Pouladi, and Laurent Longuevergne. A Comparison of Different Methods to Estimate the Effective Spatial Resolution of FO-DTS Measurements Achieved during Sandbox Experiments. Sensors, 20, 2020. ISSN 1424-8220. doi: 10.3390/s20020570.

W. Sommer, J. Valstar, P. van Gaans, T. Grotenhuis, and H. Rijnaarts. The impact of aquifer heterogeneity on the performance of aquifer thermal energy storage. Water Resources Research, 49:8128–8138, 2013. ISSN 1944-7973. doi: 10.1002/2013WR013677. URL `https://agupubs.onlinelibrary.wiley.com/doi/abs/10.1002/2013WR013677`. Number: 12.

Wei Song, Xiaoxiu Liu, Tuanfeng Zheng, and Jiaming Yang. A review of recharge and clogging in sandstone aquifer. Geothermics, 87:101857, 2020. ISSN 03756505. doi: 10.1016/j.geothermics.2020.101857.

Ruben Stemmle, Philipp Blum, Simon Schüppler, Paul Fleuchaus, Melissa Limoges, Peter Bayer, and Kathrin Menberg. Environmental impacts of aquifer thermal energy storage (ATES). Renewable and Sustainable Energy Reviews, 151, 2021. ISSN 13640321. doi: 10.1016/j.rser.2021.111560.

Károly Sztrákos and Etienne Steurbaut. Révision lithostratigraphique et biostratigraphique de l'Oligocène d'Aquitaine occidentale (France). Geodiversitas, 39:741–781, 2017. ISSN 1280-9659, 1638-9395. doi: 10.5252/g2017n4a6.

Anh-Minh Tang, Yu-Jun Cui, and Trung-Tinh Le. A study on the thermal conductivity of compacted bentonites. Applied Clay Science, 41:181–189, 2008. ISSN 0169-1317. doi: 10.1016/j.clay.2007.11.001.

S. W. Tyler, J. S. Selker, M. B. Hausner, C. E. Hatch, T. Torgersen, C. E. Thodal, and S. G. Schladow. Environmental temperature sensing using Raman spectra DTS fiber-optic methods: DTS FIBER-OPTIC SENSING. Water Resour. Res., 45, 2009. ISSN 00431397. doi: 10.1029/2008WR007052.

Nick van de Giesen, Susan C. Steele-Dunne, Jop Jansen, Olivier Hoes, Mark B. Hausner, Scott Tyler, and John Selker. Double-Ended Calibration of Fiber-Optic Raman Spectra Distributed Temperature Sensing Data. Sensors, 12:5471–5485, 2012. ISSN 1424-8220. doi: 10.3390/s120505471.

D. Vanhoudt, J. Desmedt, J. Van Bael, N. Robeyn, and H. Hoes. An aquifer thermal storage system in a Belgian hospital: Long-term experimental evaluation of energy and cost savings. Energy and Buildings, 43:3657–3665, 2011. ISSN 03787788. doi: 10.1016/j.enbuild.2011.09.040.

P.W. Visser, H. Kooi, and P.J. Stuyfzand. The thermal impact of aquifer thermal energy storage (ATES) systems: a case study in the Netherlands, combining monitoring and modeling. Hydrogeol J, 23:507–532, 2015. ISSN 1431-2174, 1435-0157. doi: 10.1007/s10040-014-1224-z. Number: 3.

Maria Vélez Márquez, Jasmin Raymond, Daniela Blessent, Mikael Philippe, Nataline Simon, Olivier Bour, and Louis Lamarche. Distributed Thermal Response Tests Using a Heating Cable and Fiber Optic Temperature Sensing. Energies, 11(11):3059, 2018. ISSN 1996-1073. doi: 10.3390/en11113059.

Bo Zhang, Kai Gu, Bin Shi, Chun Liu, Peter Bayer, Guangqing Wei, Xülong Gong, and Lei Yang. Actively heated fiber optics based thermal response test: A field demonstration. Renewable and Sustainable Energy Reviews, 134, 2020. ISSN 13640321. doi: 10.1016/j.rser.2020.110336.

Acknowledgements

This research was partly funded by the ANR project EQUIPEX CRITEX (grant number ANR-11-EQPX-0011). Jeremy Godinaud acknowleges financial and technical support by Storengy and Antea Group for technical support. Maria Klepikova acknowledges financial support by the European Union's Horizon 2020 research and innovation program under the Marie-Sklodowska Curie grant agreement No 838508.